(Received 3 July 2025, Accepted 29 August 2025, Scheduled 15 September 2025)

Compact High-Isolation Four-Port MIMO Antenna for 5G Sub-6 GHz Applications

Aziz Dkiouak[1,*], Alia Zakriti[2], Mostafa Hefnawi[3], Saad Chakkor[4], and Khalid El Khadiri[1]

[1] *STIC Laboratory, Faculty of Sciences, Chouaib Doukkali University, El Jadida, Morocco*
[2] *LabSTIC, ENSA of Tetuan, Abdelmalek Essaâdi University, Tetouan, Morocco*
[3] *Department of Electrical and Computer Engineering, Royal Military College of Canada, Kingston, ON, Canada*
[4] *LABTIC ENSA of Tangier, University of Abdelmalek Essaadi, Tangier, Morocco*

ABSTRACT: This paper presents the design and implementation of a compact 4-port MIMO antenna element with high isolation for 5G sub-6 GHz applications. Four V-shaped patch elements are arranged orthogonally on a 1.58 mm thick FR4 substrate to mitigate mutual coupling in the proposed structure. A defected ground plane method is utilized to further enhance and optimize the characteristics of the antenna at the operating frequency. The antenna operates in the 3.15–4.1 GHz frequency range, providing a 950 MHz impedance bandwidth at −10 dB, making it suitable for mobile terminals within the 5G sub-6 GHz band. The orthogonal polarization results in isolation levels below −18.1 dB, making the antenna ideal for 5G handset communications. This high isolation is reflected in an envelope correlation coefficient (ECC) of less than 0.04, while the diversity performance is verified by a total active reflection coefficient (TARC) of less than −10 dB. The channel capacity loss (CCL) of the four-port antenna element is calculated to be below 0.1 bps/Hz at 3.5 GHz. The MIMO antenna was fabricated, and its measured performance closely matches the simulated results, confirming that the proposed MIMO antenna is well suited for future sub-6 GHz cellular communications.

1. INTRODUCTION

Many cutting-edge concepts introduced in new generations of wireless communications, such as automotive radars, the intelligent internet of everything (IIoE), fifth-generation (5G) and sixth-generation (6G) wireless systems, automated industrial manufacturing, artificial intelligence (AI), autonomous vehicles, Smart Cities, Industry 4.0, and massively connected devices, all rely on multiple-input multiple-output (MIMO) antenna technologies [1–3]. These MIMO systems are organized in antenna elements at the transmitter and receiver to achieve spatial diversity, multiplexing, and beamforming techniques. This approach increases data transmission rates, system capacity, and the reliability of communication links [4]. With the growing demand for higher communication speeds and the evolving trends in modern mobile devices, antenna design must meet several key requirements, including multi-band functionality, miniaturization, and large bandwidth [5]. Mutual coupling (MC) between antenna elements is a significant factor that significantly affects the efficiency of MIMO systems. It refers to the interaction between adjacent antennas, which can cause interference and degrade the overall performance of the MIMO system by reducing spatial diversity, increasing signal correlation, and reducing channel capacity [6]. Numerous strategies have been proposed to reduce MC in MIMO systems. The authors in [7–9] introduced slot insertion techniques in antennas to achieve high isolation. These solutions reduce the signal's wavelength near antennas, increasing their electrical separation. Other methods employ cross-shaped decoupling structures [10] or T-shaped slots [11] to improve the isolation between antenna elements. The neutralization line has also been employed to prevent the mutual coupling in the structure created by antenna ports. These techniques are used with planar inverted F-shape antennas (PIFAs) [12] and printed monopole antennas [13]. In [14], electromagnetic bandgap (EBG) structures were proposed to minimize the MC by suppressing surface waves. In [15], the hybrid technique has been suggested to minimize mutual coupling within the proposed structure. In [16], Anuar et al. presented a triple band MIMO antenna for long term evolution (LTE) applications using dielectric resonator antenna (DRA). In [17], a 4-port flexible MIMO antenna with isolation enhancement for wireless internet of things (IoT) applications has been proposed by Azimov et al. In [18], a high isolation multiband MIMO antenna structure for WLAN/WiMAX/5G applications using orthogonal orientation has been analyzed by Dileepan et al.

This paper proposes a compact antenna element design for 5G mobile telephony in the 3.5 GHz band. The system comprises four compact patch antennas mounted on a printed circuit board (PCB). The defective ground plane technique achieves good radiation in both directions and improves impedance matching at the resonant frequency. The positioning and alignment of each patch on the PCB's upper surface play a critical role in enhancing isolation, thereby reducing the correlation between the antennas.

The remainder of the paper is organized as follows. Section 2 details the design of the proposed MIMO antenna for mobile terminals operating in the 5G Sub-6 GHz band. Sec-

* Corresponding author: Aziz Dkiouak (dkiouak.aziz@ucd.ac.ma).

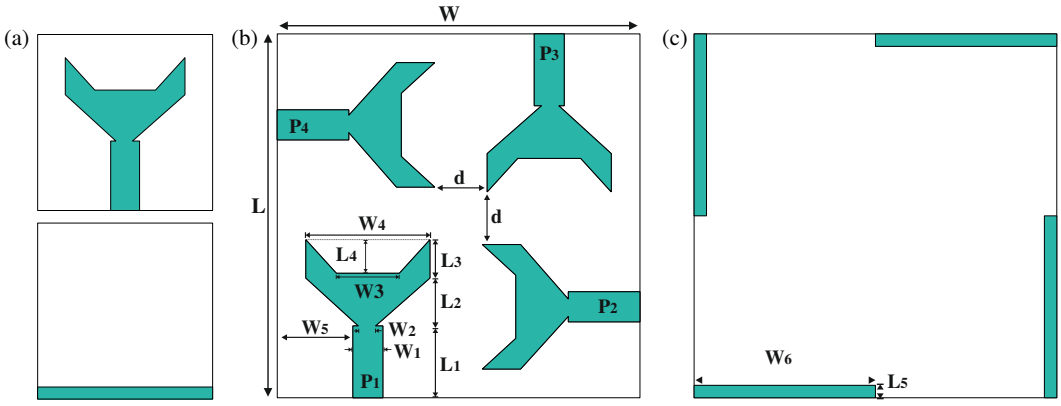

FIGURE 1. MIMO antenna design: (a) one-element cell, (b) top side of four-element and (c) bottom side of four-element.

tion 3 presents the simulation results for various parameters of the proposed antenna. Section 4 discusses the fabrication, testing, and analysis of the structure, with its functionality validated through experimentation within the specified operating frequency range. Section 5 compares the proposed MIMO antenna with other recent research efforts. Finally, Section 6 provides the conclusion. The benefits of the proposed structure are summarized as follows:

(i) Cost-effective substrate and compactness structure: The MIMO antenna has been manufactured on a compact size with a low-loss FR-4 substrate, providing a cost-effective solution that maintains good performances. This makes it suitable for the integration in mobile terminals and portable 5G devices.

(ii) High isolation: The design achieves a level of isolation that exceeds -18.1 dB through the use of orthogonal polarization and a defected ground structure. This minimizes mutual coupling on the studied structure.

(iii) Wide bandwidth: The antenna covers a wide bandwidth, covering the 3.15–4.1 GHz band with a bandwidth of **950 MHz**, thus supporting the sub-6 GHz 5G applications.

(iv) Good diversity performance: The simulated envelope correlation coefficient (**ECC** $<$ **0.04**) and diversity gain (**DG** $>$ **9.97 dB**) ensure strong multipath diversity for reliable communication.

(v) Improved system efficiency: The proposed MIMO antenna provides about 60% radiation efficiency and a gain of 3.63 dBi, sufficient for mobile communication.

(vi) Validated design: The fabricated prototype and experimental measurements closely match simulations, confirming practical feasibility.

2. SINGLE AND FOUR PORT ANTENNA ELEMENT CONFIGURATIONS

2.1. One-Element Cell

The antenna design begins with a rectangular patch element printed on the top surface of the substrate, while a full ground plane is placed on the opposite side. To improve the performance of this initial configuration, geometric modifications are introduced on both the radiating monopole and the ground plane, as shown in Figure 1(a). Using Computer Simulation Technology (CST) Microwave Studio, parametric optimization is carried out to achieve improved impedance bandwidth and radiation characteristics. A narrow backing ground plane with dimensions W_6 and L_5 is adopted, as it modifies the surface current distribution and introduces additional resonance paths compared with a full ground plane. This modification leads to good radiation in both directions and better impedance matching at the resonant frequency, as shown in Figure 2.

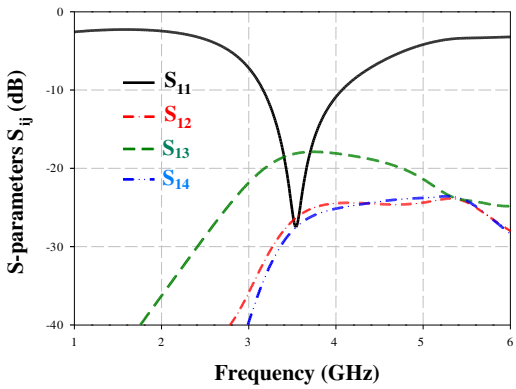

FIGURE 2. Simulation of S-parameter curve.

2.2. Four-Port Antenna Element Configurations

The proposed antenna element is built on two sides of an FR4 substrate, with a thickness of 1.58 mm, a dielectric constant of $\varepsilon_r = 4.4$, and a loss tangent $\tan\delta = 0.02$. The inexpensive cost of this substrate compared to other substrate materials is its defining feature. Each antenna has a microstrip feed line for power supply and is shaped like a square. A simple rectangular structure is added at the bottom to ensure good radiation in both directions. The positioning of every antenna on the dielectric substrate is altered. Each antenna is initially centered on its designated ground, and its orientation is adjusted relative to the other antennas. For inter-element spacing less than $\frac{\lambda}{2}$, it is shown that a specific antenna rotation helps to maximize

TABLE 1. Optimized four-port MIMO antenna parameters.

Parameters	W	L	L_1	L_2	L_3	L_4	L_5	W_1	W_2	W_3	W_4	W_5	W_6	D
Values (mm)	38	38	7.5	5	4	3.5	1.3	3.14	1.8	6.6	13	8	19	5.5

polarization diversity and reduce MC between the antenna components. Using this technique, we create a small structure with less mutual coupling, which lowers the correlation of the signals arriving at each antenna in the element. The final structure is shown in Figure 1. It consists of four antennas, labeled $P1$, $P2$, $P3$, and $P4$, arranged symmetrically and orthogonally to one another, with a spacing of $d = 38$ mm. The optimized antenna parameters for this structure are provided in Table 1.

3. SIMULATION RESULTS

3.1. S-Parameters and Surface Current Distribution

CST (Computer Simulation Technology) Microwave Studio software was used to design and analyze this antenna. The S-parameters are given in Figure 2. Due to symmetry, only S_{11}, S_{12}, S_{13}, and S_{14} are shown. The reflection coefficient S_{11} describes the ratio between the input and output ports and indicates the amount of power reflected by the antenna. This factor is below 28 dB at 3.5 GHz with an impedance bandwidth of 950 MHz (3.15 to 4.1 GHz), consistent with the required reflection coefficient for 5G mobile telephony. On the same plot, the minimum isolation among the four ports is more than -18.1 dB at the resonance frequency of 3.5 GHz. This indicates the excellent response of the polarization diversity employed in this design.

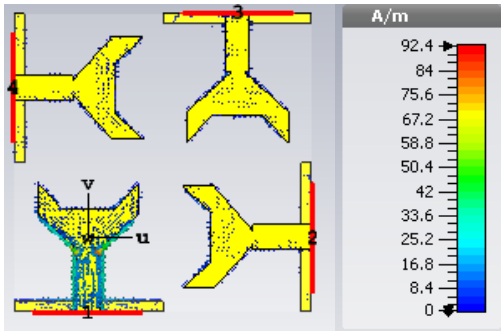

FIGURE 3. Current distribution on the surface of the four elements from port 1 at 3.5 GHz.

Figure 3 depicts the surface currents distribution of the proposed structure, emanating from port 1 at the resonant frequency of 3.5 GHz. This figure demonstrates that the current density is the greatest near the excited line, with a high current density of 92.4 A/m at 3.5 GHz. Polarization diversity has a significant impact, as it prevents current from flowing to the adjacent patch elements, thus reducing the effect of MC and increasing the radiation efficiency.

3.2. Envelope Correlation Coefficient (ECC) and Diversity Gain (DG)

The calculation of the envelope correlation coefficient (ECC) for the ith and jth antenna elements using 3D radiation patterns can be performed as follows [19]:

$$ECC(i,j) = \frac{\left(\oint \left(X_{PR}E_{\theta i}(\Omega)E^*_{\theta j}(\Omega)P_\theta(\Omega) + E_{\varphi i}(\Omega)E^*_{\varphi j}(\Omega)P_\varphi(\Omega)\right) d(\Omega)\right)^2}{\oint (X_{PR}G_{\theta i}(\Omega)P_\theta(\Omega)+G_{\varphi i}(\Omega)P_\varphi(\Omega))d(\Omega) \cdot \oint (X_{PR}G_{\theta j}(\Omega)P_\theta(\Omega)+G_{\varphi j}(\Omega)P_\varphi(\Omega))d(\Omega)}, \quad (1)$$

where X_{PR} designates the cross-polarization power ratio of the spreading region; $G_\theta(\Omega) = E_\theta(\Omega)E^*_\theta(\Omega)$ is the power pattern of θ polarization; and $G_\varphi(\Omega) = E_\varphi(\Omega)E^*_\varphi(\Omega)$ is the power pattern of φ polarizations. $P_\theta(\Omega)$ designates the angular density functions of the θ polarization, and $P_\varphi(\Omega)$ denotes the angular density function of the ϕ polarization. $E_{\theta i}(\Omega)$ and $E_{\theta j}(\Omega)$ are the electric field patterns of the ith and jth antenna elements in the θ polarization, respectively. $E_{\varphi i}(\Omega)$ and $E_{\varphi j}(\Omega)$ are the electric field patterns of the ith and jth antenna elements in the φ polarization, respectively. In a 4×4 MIMO system, the ECCs are shown in Figure 4(a) and denoted as $ECC(i,j)$.

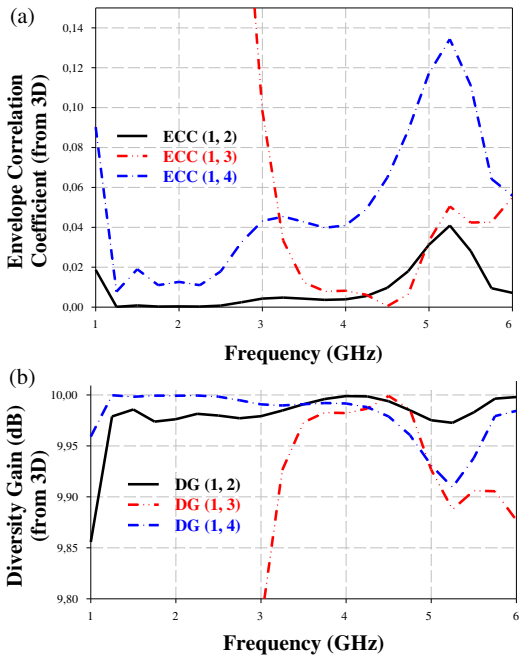

FIGURE 4. Far-field ECC and DG curves: (a) ECC and (b) DG.

The diversity gain, DG, may be computed from the ECC using [20]

$$DG = 10\sqrt{\left(1 - |\rho|^2\right)}, \quad (2)$$

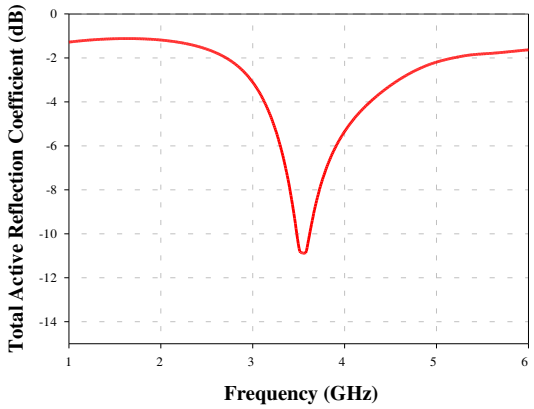

FIGURE 5. Simulated TARC curve.

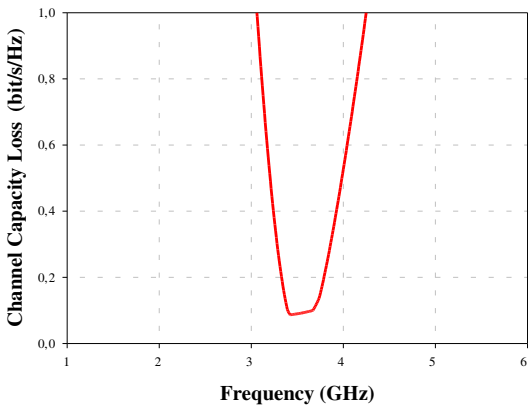

FIGURE 6. Simulated CCL curve.

where ρ is the coefficient of complex cross-correlation, and $|\rho|^2 = ECC$.

Figure 4 shows ECC and DG values for the four antennas based on their 3D radiation patterns. As seen in Figure 4(a), the magnitude of ECCs at 3.5 GHz is less than 0.04. This is well below the threshold of 0.5, indicating excellent diversity performance. This can be attributed to the high isolation among the four elements and the achieved polarization diversity. Consequently, the DG values exceed 9.97 at 3.5 GHz, as shown in Figure 4(b).

3.3. Total Active Reflection Coefficient (TARC) and Channel Capacity Loss (CCL)

The total active reflection coefficient (TARC) is a parameter that accurately characterizes the efficiency and bandwidth of the MIMO technology. TARC can be calculated using S-parameters [21, 22]. The total active reflection coefficient for a 4-element antenna element is calculated according to [23, 24] as follows

$$TARC = \frac{\sqrt{\begin{array}{l}\left|S_{11}+S_{12}e^{j\theta}+S_{13}e^{j\theta'}+S_{14}e^{j\theta''}\right|^2 \\ +\left|S_{21}+S_{22}e^{j\theta}+S_{23}e^{j\theta'}+S_{24}e^{j\theta''}\right|^2 \\ +\left|S_{31}+S_{32}e^{j\theta}+S_{33}e^{j\theta'}+S_{34}e^{j\theta''}\right|^2 \\ +\left|S_{41}+S_{42}e^{j\theta}+S_{43}e^{j\theta'}+S_{44}e^{j\theta''}\right|^2\end{array}}}{2} \quad (3)$$

where θ, θ', and θ'' are the phase differences between excitation ports.

Figure 5 presents the TARC values generated by taking nine random phase combinations (θ, θ', and θ'') and averaging their results. In a communication system, the TARC value of an antenna should be less than -10 dB. The chart demonstrates that the proposed antenna element performs well, as the average simulated TARC within the operational frequency band is consistently below -10 dB.

Another important metric for evaluating the performance of MIMO antennas is channel capacity loss (CCL), expressed in bits/s/Hz. It represents the rate at which data is transmitted through a communication link [21]. CCL value should be below 0.4 bits/s/Hz to ensure optimal performance [18]. The CCL of a four-port MIMO antenna is defined mathematically by [25]

$$CCL = -\log_2 \det\left(\psi^R\right) \quad (4)$$

where ψ^R is the correlation matrix of the receiving antennas given by

$$\psi^R = \begin{bmatrix} \rho_{11} & \rho_{12} & \rho_{13} & \rho_{14} \\ \rho_{21} & \rho_{22} & \rho_{23} & \rho_{24} \\ \rho_{31} & \rho_{32} & \rho_{33} & \rho_{34} \\ \rho_{41} & \rho_{42} & \rho_{43} & \rho_{44} \end{bmatrix} \quad (5)$$

where the correlation *matrix* coefficients ρ_{ii} and ρ_{ij} are given by $\rho_{ii} = 1 - |\sum_{n=1}^{M} S_{in}^* \times S_{ni}|$ and $\rho_{ij} = -\sum_{n=1}^{M} S_{in}^* \times S_{nj}$ for $ij = 1, 2, 3,$ and 4.

Figure 6 presents the simulated CCL performance results, calculated from Equations (4) and (5). Within the operating band, a value of less than 0.1 bits/s/Hz is achieved.

3.4. Gain and Total Radiation Efficiency

Figures 7 and 8 show the radiation efficiency and maximum gain of the antenna element, respectively. The radiation efficiency follows a similar trend to the gain. The simulated gain is 3.63 dBi, and the efficiency is approximately 60% within the required frequency band, ensuring minimal power dissipation through ohmic losses. This value is well within acceptable limits for practical applications.

4. TEST RESULTS AND APPLICATION

To validate the performance of the proposed antenna element, a prototype has been manufactured as shown in Figure 9 and tested. The fabrication process and measurements were carried out at the Intelligent System Design Laboratory of AbdelMaleK Essaâdi University (AEU). The fabrication is performed using LPKF Protomat E33 printed circuit board milling machine.

4.1. Measurement Results

Our analysis is based on measurements at a 3.5 GHz frequency band using a Rohde and Schwarz ZVB 20 vector network ana-

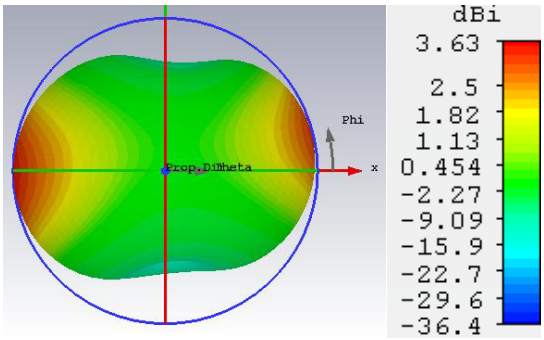

FIGURE 7. Simulation of 3D radiation patterns at 3.5 GHz.

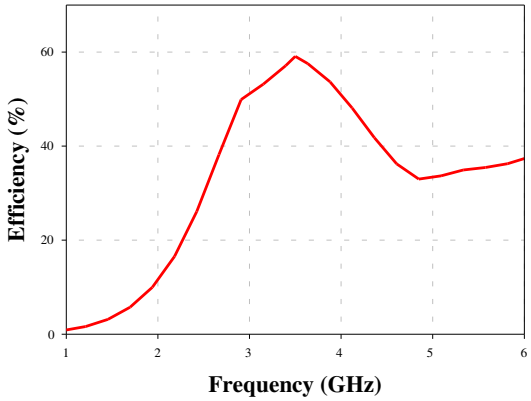

FIGURE 8. Simulated efficiency curve.

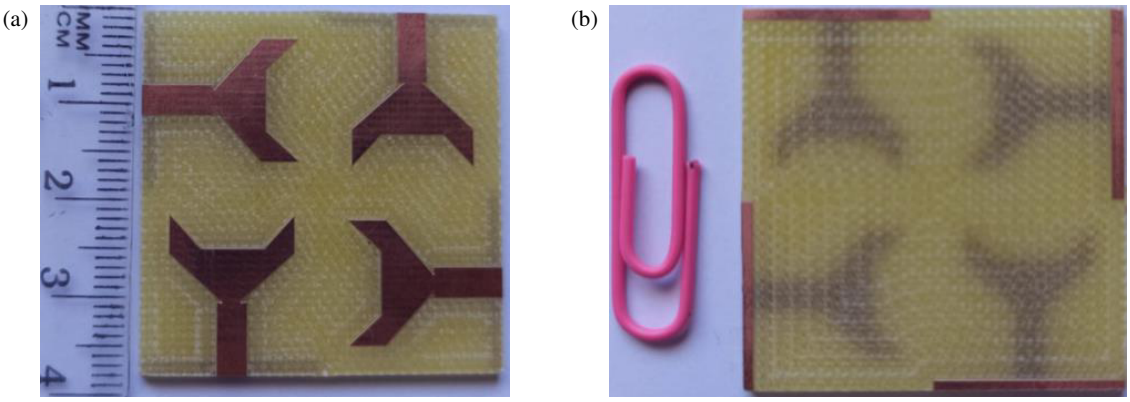

FIGURE 9. Pictures of the fabricated structure: (a) front photo and (b) back photo.

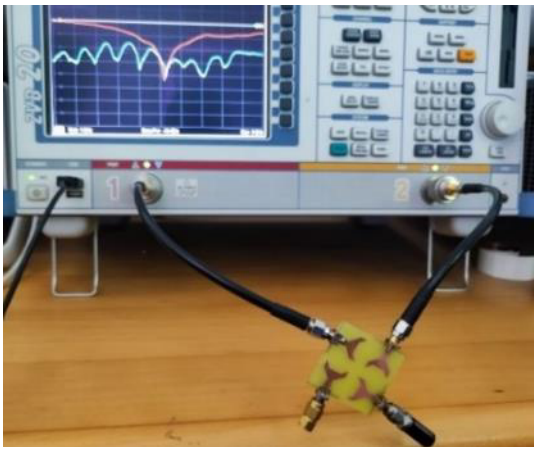

FIGURE 10. S-parameters measurement.

lyzer, as shown in Figure 10. In a MIMO system, when the ith port is powered, the others are ended with 50 Ω.

Figure 11 presents the measured and simulated return losses and mutual coupling. Figure 11(a) compares the measured and simulated return loss parameters, S_{ii}. Despite a shift in the resonance frequency, the measured return loss still exceeds −24 dB at the resonance frequency of 3.5 GHz. The discrepancies between the measured and simulated return losses could be attributed to SMA connector losses, fabrication errors, parasitic effects, and physical characteristics of the PCB material used in fabrication. Figure 11(b) compares the measured and simulated mutual coupling, S_{ii}. It is observed that the measured mutual coupling has been significantly reduced, reaching a value of −24 dB.

4.2. Radiation Pattern

Radiation pattern measurements were conducted within a non-anechoic chamber with the use of the Geozondas kit, as illustrated in Figure 12. The transmitter was a horn antenna at the focal point of a reflector to change spherical into plane waves, which were then directed towards the antenna under test (AUT) in receiving mode.

The measured and simulated normalized radiation patterns for the four elements are shown in Figure 13. The radiation patterns are plotted for two planes, H-plane (xoz-plane) and E-plane (xoy-plane), at a frequency of 3.5 GHz. The results show a consistent radiation pattern across the frequency band, with a strong correlation between the measured and simulated radiation patterns. The E-plane radiation pattern of the designed structure forms an "8" shape at 3.5 GHz. This indicates that the structure provides bidirectional radiation in the E-plane with the orthogonal placement of the four elements. The co-polarization radiation patterns in the H-plane are nearly omnidirectional, forming an "O" shape. Although there is a high

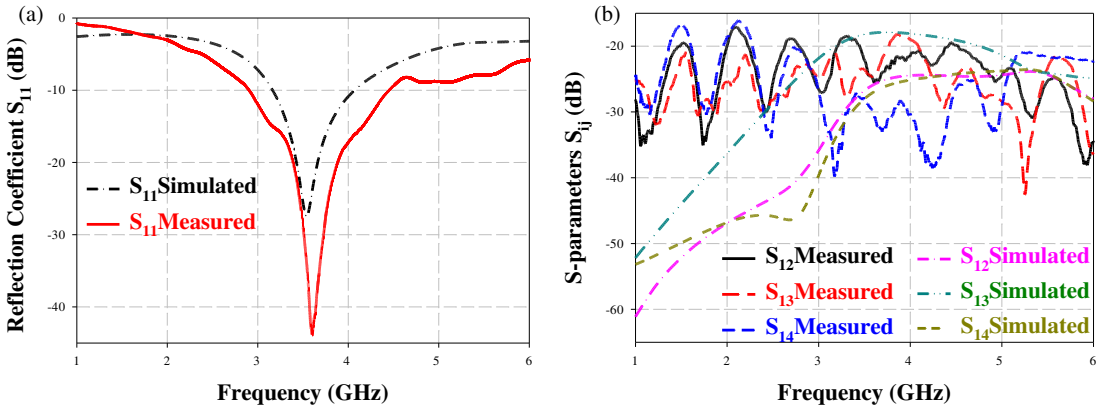

FIGURE 11. Measurement results: (a) S_{ii} and (b) S_{ij}.

FIGURE 12. Radiation pattern measurements using the Geozondas kit.

TABLE 2. Result comparison between the work presented and other new MIMO antennas.

Ref. No.	Size in term of (mm^2 and λ_0)	Isolation (dB)	Design Type	Efficiency (%)	Gain (dBi)	ECC	CCL (bits/Hz)	TARC (dB)	Substrate
This work	$38 \times 38 = 1444$ $0.4\lambda_0 \times 0.4\lambda_0$	-18.1	Orthogonal polarization	60	3.63	0.4	< 0.1	< -10	FR-4
[26]	$150 \times 75 = 11250$ $1.7\lambda_0 \times 0.85\lambda_0$	-16	CPW-Fed Diversity	65–80	3.6 dB	0.005	–	< -10	FR-4
[24]	$58 \times 58 = 3364$ $0.06\lambda_0 \times 0.06\lambda_0$	-17	Hybrid method (DGS & Windmill-Shaped)	50.1 (-3 dB)	4.3	0.04	< 0.6	< -10	FR-4
[27]	$80 \times 80 = 6400$ $0.9\lambda_0 \times 0.9\lambda_0$	-15	Metamaterial	—	5.2 dB	—	—	—	RT 8850
[28]	$136 \times 68.8 = 9356.8$ $1.6\lambda_0 \times 0.8\lambda_0$	-11	Open-end slot	50–60	3	0.15	—	—	FR-4
[29]	$67 \times 138 = 9246$ $0.8\lambda_0 \times 1.66\lambda_0$	-15	Orthogonal adjustment	—	–	0.005	< 0.19	—	RT 5880
[30]	$110 \times 110 = 12100$ $0.62\lambda_0 \times 0.62\lambda_0$	-20	Hybrid method (Orthogonal & Slots)	90	5.2	0.0025	—	< -10	FR-4
[31]	$40 \times 40 = 1600$ $0.64\lambda_0 \times 0.64\lambda_0$	-25	Orthogonal adjustment	70	2.8	0.01	—	–	FR-4
[16]	$23.5 \times 83 = 1950.5$ $0.02\lambda_0 \times 0.7\lambda_0$	-30.5	Orientation	85	1 dB	0.001	< 0.4	< -10	FR-4
[14]	$100 \times 100 = 10000$ $0.06\lambda_0 \times 0.06\lambda_0$	-20	DRA slot	—	5.5	0.02	—	—	FR-4

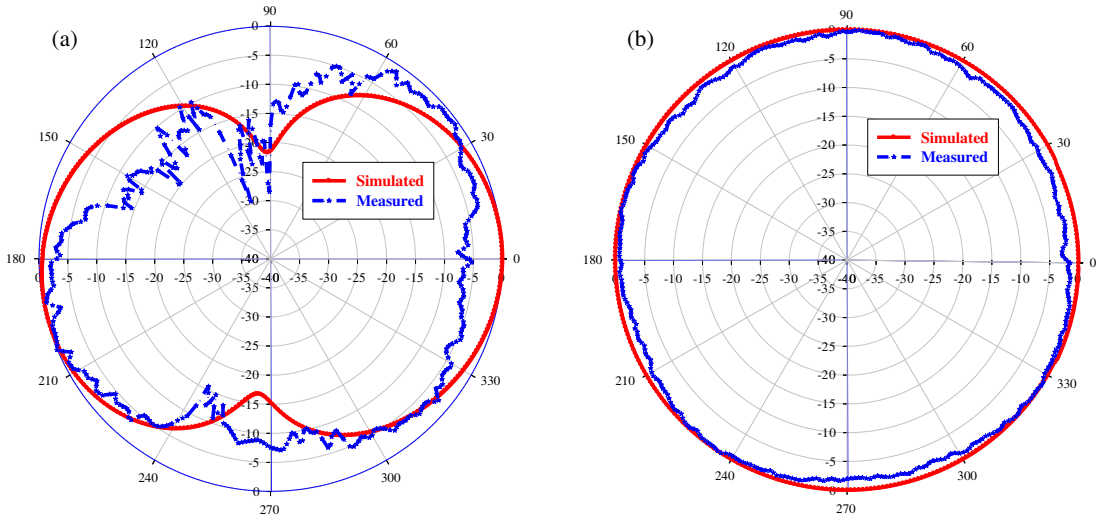

FIGURE 13. Simulated and measured radiation patterns at 3.5 GHz: (a) E-plane and (b) H-plane.

level of cross-polarization, it does not impact the performance of the MIMO antenna, as the propagation paths in mobile wireless communication typically involve multipath propagation in the H-plane.

5. PERFORMANCE COMPARISON

Table 2 compares the performance of our work to other similar studies. The proposed MIMO antenna system demonstrates a compact size and lower mutual coupling than other designs, while maintaining comparable efficiency and gain.

6. CONCLUSION

This paper proposes a simple and compact four-element antenna for 5G mobile telephony. By employing orthogonal polarization and a defective ground plane, the design achieves a compact size of $38 \times 38\,\text{mm}^2$, an impedance bandwidth of 27.14%, isolation below -18.1 dB, a gain of 3.63 dBi, and an efficiency of 60%. Regarding radiation and MIMO diversity, the antenna also demonstrates strong performance, with an ECC less than 0.04, a DG greater than 9.97 dB, a TARC below -10 dB, and CCL values under 0.1 at 3.5 GHz. Both experimental and simulated results were conducted, and their performances were compared to validate the proposed MIMO antenna's suitability for 5G applications in the sub-6 GHz range.

REFERENCES

[1] Omondi, G. and T. O. Olwal, "Towards artificial intelligence-aided MIMO detection for 6G communication systems: A review of current trends, challenges and future directions," *e-Prime — Advances in Electrical Engineering, Electronics and Energy*, Vol. 6, 100376, 2023.

[2] El Ahmar, L., A. Errkik, J. Zbitou, A. Oukaira, I. Bouzida, L. Talbi, and A. Lakhssassi, "A compact meander flexible UHF tag for industrial applications," *e-Prime — Advances in Electrical Engineering, Electronics and Energy*, Vol. 7, 100402, 2024.

[3] Omondi, G. and T. O. Olwal, "Variational autoencoder-enhanced deep neural network-based detection for MIMO systems," *e-Prime — Advances in Electrical Engineering, Electronics and Energy*, Vol. 6, 100335, 2023.

[4] Almalki, M. H., A. Affandi, and A. Syed, "Design of dual-band, 4-ports MIMO antenna-diplexer based on quarter-mode substrate integrated waveguide," *International Journal of Antennas and Propagation*, Vol. 2022, No. 1, 4151038, 2022.

[5] Bojkovic, Z. and D. Milovanovic, "A technology vision of the fifth generation (5G) wireless mobile networks," in *International Conference on Emerging Trends in Electrical, Electronic and Communications Engineering*, Vol. 416, 25–43, Springer, Cham, 2016.

[6] El Bakali, H. E. O., A. Zakriti, A. Farkhsi, A. Dkiouak, and M. E. Ouahabi, "Design and realization of dual band notch UWB MIMO antenna in 5G and Wi-Fi 6E by using hybrid technique," *Progress In Electromagnetics Research C*, Vol. 116, 1–12, 2021.

[7] Salim, N., M. S. J. Singh, A. T. Abed, and M. T. Islam, "4 × 4 MIMO slot antenna spanner shaped low mutual coupling for Wi-Fi 6 and 5G communications," *Alexandria Engineering Journal*, Vol. 78, 141–148, 2023.

[8] Rahman, M. A., S. S. Al-Bawri, W. M. Abdulkawi, K. Al-jaloud, and M. T. Islam, "A unique SWB multi-slotted four-port highly isolated MIMO antenna loaded with metasurface for IOT applications-based machine learning verification," *Engineering Science and Technology, An International Journal*, Vol. 50, 101616, 2024.

[9] Chakraborty, S., M. A. Rahman, M. A. Hossain, E. Nishiyama, and I. Toyoda, "A novel dual-band elliptical ring slot MIMO antenna with orthogonal circular polarization for 5G applications," *Heliyon*, Vol. 10, No. 13, e33176, 2024.

[10] Alfakhri, A., "Dual polarization and mutual coupling improvement of UWB MIMO antenna with cross shape decoupling structure," *e-Prime — Advances in Electrical Engineering, Electronics and Energy*, Vol. 4, 100130, 2023.

[11] Addepalli, T. and V. R. Anitha, "A very compact and closely spaced circular shaped UWB MIMO antenna with improved isolation," *AEU — International Journal of Electronics and Communications*, Vol. 114, 153016, 2020.

[12] Fritz-Andrade, E., R. Gomez-Villanueva, J. A. Tirado-Méndez, L. A. Vasquez-Toledo, A. Rangel-Merino, and H. Jardon-Aguilar, "Broadband four elements PIFA array for access-point MIMO systems," *Progress In Electromagnetics Research C*, Vol.

106, 163–176, 2020.

[13] Dkiouak, A., M. E. Ouahabi, S. Chakkor, M. Baghouri, A. Zakriti, and Y. Lagmich, "High performance UWB MIMO antenna by using neutralization line technique," *Progress In Electromagnetics Research C*, Vol. 131, 185–195, 2023.

[14] Fadehan, G. A., Y. O. Olasoji, and K. B. Adedeji, "Mutual coupling effect and reduction method with modified electromagnetic band gap in UWB MIMO antenna," *Applied Sciences*, Vol. 12, No. 23, 12358, 2022.

[15] Mchbal, A., N. A. Touhami, H. Elftouh, and A. Dkiouak, "Isolation enhancement using a hybrid technique in an eight-element UWB MIMO antenna design," *Advanced Electromagnetics*, Vol. 9, No. 3, 56–65, 2020.

[16] Anuar, S. U., M. H. Jamaluddin, J. Din, K. Kamardin, M. H. Dahri, and I. H. Idris, "Triple band MIMO dielectric resonator antenna for LTE applications," *AEU — International Journal of Electronics and Communications*, Vol. 118, 153172, 2020.

[17] Azimov, U. F., A. Abbas, S.-W. Park, N. Hussain, and N. Kim, "A 4-port flexible MIMO antenna with isolation enhancement for wireless IoT applications," *Heliyon*, Vol. 10, No. 11, e32216, 2024.

[18] Dileepan, D., S. Natarajan, and R. Rajkumar, "A high isolation multiband MIMO antenna without decoupling structure for WLAN/WiMAX/5G applications," *Progress In Electromagnetics Research C*, Vol. 112, 207–219, 2021.

[19] Dkiouak, A., M. E. Ouahabi, A. Zakriti, S. Chakkor, and M. Baghouri, "Design of four-element MIMO antenna system for Intelligent Internet of Everything (IIoE)," *Telecommunication Systems*, Vol. 86, No. 3, 559–570, 2024.

[20] Beniysa, M., A. Dkiouak, A. E. J. E. Idrissi, A. Zakriti, and M. E. Ouahabi, "Design and performance of a compact two inset-fed patch MIMO antenna for 5G networks," in *International Conference Interdisciplinarity in Engineering*, Vol. 605, 828–835, Springer, Cham, 2022.

[21] Munir, M. E., M. M. Nasralla, and M. A. Esmail, "Four port tri-circular ring MIMO antenna with wide-band characteristics for future 5G and mmWave applications," *Heliyon*, Vol. 10, No. 8, e28714, 2024.

[22] Elalaouy, O., M. E. Ghzaoui, and J. Foshi, "Mutual coupling reduction of a two-port MIMO antenna using defected ground structure," *e-Prime — Advances in Electrical Engineering, Electronics and Energy*, Vol. 8, 100557, 2024.

[23] Khalid, M., S. I. Naqvi, N. Hussain, M. Rahman, Fawad, S. S. Mirjavadi, M. J. Khan, and Y. Amin, "4-port MIMO antenna with defected ground structure for 5G millimeter wave applications," *Electronics*, Vol. 9, No. 1, 71, 2020.

[24] Yu, C., S. Yang, Y. Chen, W. Wang, L. Zhang, B. Li, and L. Wang, "A super-wideband and high isolation MIMO antenna system using a windmill-shaped decoupling structure," *IEEE Access*, Vol. 8, 115 767–115 777, 2020.

[25] Achariparambil, A., K. K. Indhu, R. A. Kumar, K. Neema, and C. K. Aanandan, "Ultra-wideband quad element MIMO antenna on a flexible substrate for 5G and wearable applications," *Progress In Electromagnetics Research C*, Vol. 126, 143–155, 2022.

[26] Ojaroudi Parchin, N., H. J. Basherlou, Y. I. A. Al-Yasir, A. M. Abdulkhaleq, M. Patwary, and R. A. Abd-Alhameed, "A new CPW-fed diversity antenna for MIMO 5G smartphones," *Electronics*, Vol. 9, No. 2, 261, 2020.

[27] Ali, F., M. Salih, and M. Ilyas, "MIMO patch antenna with metamaterial 3.5 GHz for 5G applications," in *2022 Second International Conference on Advances in Electrical, Computing, Communication and Sustainable Technologies (ICAECT)*, 1–4, Bhilai, India, 2022.

[28] Abdullah, M., S. H. Kiani, L. F. Abdulrazak, A. Iqbal, M. A. Bashir, S. Khan, and S. Kim, "High-performance multiple-input multiple-output antenna system for 5G mobile terminals," *Electronics*, Vol. 8, No. 10, 1090, 2019.

[29] Jamshed, M. A., M. Ur-Rehman, J. Frnda, A. A. Althuwayb, A. Nauman, and K. Cengiz, "Dual band and dual diversity four-element MIMO dipole for 5G handsets," *Sensors*, Vol. 21, No. 3, 767, 2021.

[30] Tirado-Méndez, J. A., H. Jardón-Aguilar, A. Rangel-Merino, L. A. Vasquez-Toledo, and R. Gómez-Villanueva, "Four ports wideband drop-shaped slot antenna for MIMO applications," *Journal of Electromagnetic Waves and Applications*, Vol. 34, No. 9, 1159–1179, 2020.

[31] Ali, H., X.-C. Ren, I. Bari, M. A. Bashir, A. M. Hashmi, M. A. Khan, S. I. Majid, N. Jan, W. U. K. Tareen, and M. R. Anjum, "Four-port MIMO antenna system for 5G n79 band RF devices," *Electronics*, Vol. 11, No. 1, 35, 2022.